

Fractal Analysis of AFM Images of Worn-Out Contact Lens Inner Surface

Božica Bojović

Research Assistant
University of Belgrade
Faculty of Mechanical Engineering

Zoran Miljković

Associate Professor
University of Belgrade
Faculty of Mechanical Engineering

Bojan Babić

Full Professor
University of Belgrade
Faculty of Mechanical Engineering

The interest in biomaterials surface technology has led to an investigation of rigid gas permeable contact lens inner surface using scanning probe microscopy for measurement. Topography and phase images were recorded in order to investigate surface roughness and properties after an extended period of contact lens wearing. Analysis is based on fractal approach incorporated with MatLab software for image processing. The fractal dimension, calculated by skyscrapers method, is used for surface identification and subsequently for surface behaviour explanation. The authors' aim is to point out that time is merely a commercial category for rigid gas permeable contact lens replacement and that only significant changes in surface properties render such replacement necessary.

Keywords: fractals, topography, surface, AFM, image.

1. INTRODUCTION

There is no strong recommendation for rigid gas permeable contact lens (RGP CL) wear period, and wearer's determine the end-stage, e.g. when they notice either vision deterioration or unpleasant sense while wearing. CL can lose functionality due to accumulated proteins, lipids, and other tear components on CL surface, despite routine cleaning activities. Additionally, every single RGP CL wearer provides unique ambient conditions in which these CL biosurfaces have to function, resulting in an individual CL end-stage period. Since CL surfaces become significantly rougher after prolonged wear, they become more prone to bacterial adhesion and protein and lipid deposits. The recommended schedule has to take into account the moment when surface roughness exceeds a critical limit.

The paper describes usefulness of topography and phase images analysis application in the RGP CL replacement schedule. The loss of RGP CL functionality has to be investigated and related to measurable parameters in order to recommend replacement based on "hard evidence" instead of time. The period of use cannot be a commercial category for RGP CL replacement but should be associated with significant changes in surface properties.

There is no clear answer to the question as to what surface standard parameter should be used for critical limit determination. The result of the study, reported in [1], also confirms the need for the replacement schedule of RGP CL. The water contact angle, percentage of elemental surface composition and deposit rate of bacteria was related to standard average roughness parameter Ra. It was stated in [2] that surface roughness was the most influential lens surface property after 10 days of wear.

This paper focuses on the quantification of the textures of CL inner surface by applying a method

differing from the standard parameters characterizations, because single standard parameter fails to describe functional nature of the surface, and use of more than one roughness parameter exhibits more shortcomings. This is mainly due to the partial information contained in each descriptor.

Authors belong to the group of researchers who prefer fractal parameter characterization that enables to distinguish surfaces, compare them and predict functional behaviour in use. Fractal analysis was used in [3] for quantitative characterizations of grinded ceramics surface textures by surface profile fractal dimension. Fractal analysis of biomedical surface topography, as an extent of previous research efforts, is influenced by growing interest in biomaterials surface technology. Fractal geometry provides a useful tool for the analysis of complex and irregular structures such as biomedical surface topography based on image analysis methods that consider an image as a 3D surface. In this paper the "skyscrapers" method is chosen for calculating fractal dimension of surface based on [4]. This method presupposes surface recording as an image, by using scanning probe microscopy (SPM).

2. THE WORN-OUT RGP CL PROBLEM STATEMENT

The sample is a RGP CL made of ML 92 Siflufocan A, and shown in Figure 1, placed on cornea. This lens is worn by 37 year-old female over an extended period (in fact more than 5 years) of regular use and storage. The wearer reported unpleasant sense during the wearing, namely lens sliding across cornea. The ophthalmologist pointed out that there was no vision deterioration but there is an obvious fast sliding process accompanied by occurrence of air bubble, which can be observed in Figure 1. Figure 1 is a capture from the video record made by using optometric device for cornea parameter measurement and contact lens control.

This RGP CL is "worn out" and replaced due to change of some surface properties that caused low adhesion between inner surface and tear film. The adhesion force holds the RGP lens in the eye. The appropriate adhesion force amount obtained by

Received: November 2008, Accepted: December 2008

Correspondence to: Božica Bojović, M.Sc.

Faculty of Mechanical Engineering,

Kraljice Marije 16, 11120 Belgrade 35, Serbia

E-mail: bbojovic@mas.bg.ac.rs

manufacturing process, consisting of turning with polishing as finishing process, is shown in Figure 2.

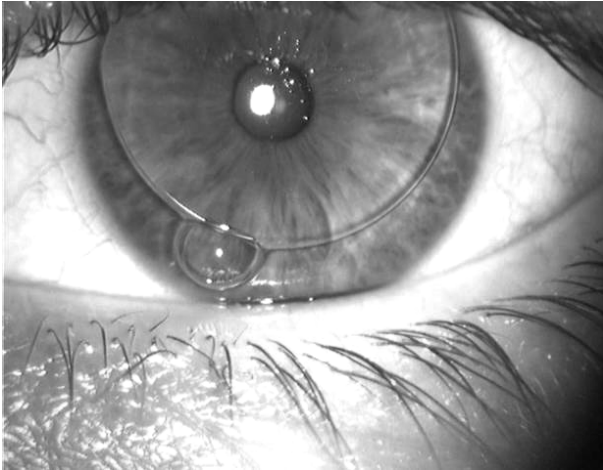


Figure 1. RGP CL placed on cornea with air bubble on its edge

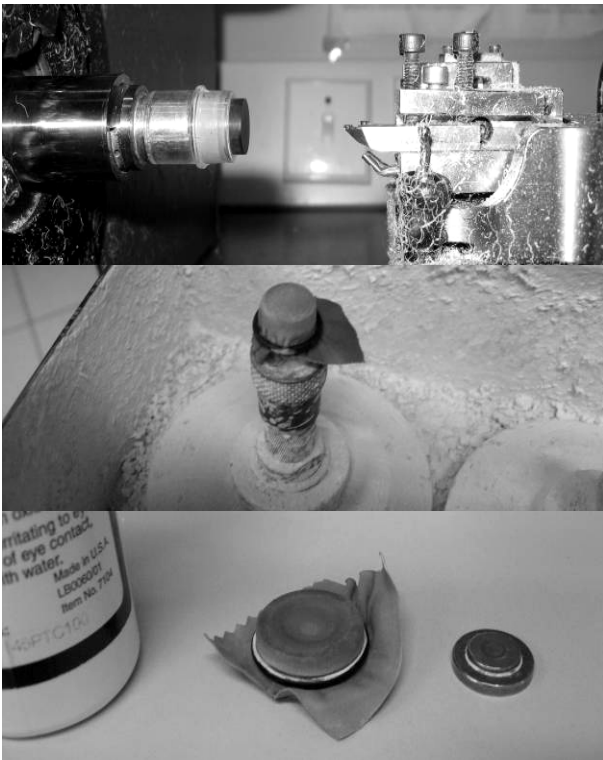


Figure 2. Stages of RGP CL manufacturing process – diamond turning and polishing

The double side turning with diamond tools for coarse and fine operations also includes axial edge lift (AEL) operation. The side-cutting edge angle of diamond tool is $\psi = 60^\circ$ and nose radius is $R = 0.25$ mm. The depth of cut for coarse turning and AEL operations is $a_c = 0.4$ mm and angular feed is $\theta_c = 6^\circ/s$. Depth of cut for fine turning is $a_f = 0.05$ mm and angular feed is $\theta_f = 2^\circ/s$. The rotational speed during turning process is $n = 8000$ rev/min. The natural rubber (caoutchouc) polishing tool is moulded with sphere radius decreased by fibre patch thickness. The polishing paste contains aluminium oxide particles sized from $0.3 \mu\text{m}$ to $0.5 \mu\text{m}$. The duration of polishing ($10 \div 15$ s) determines surface quality, that is to say surface roughness, and consequently the adhesion.

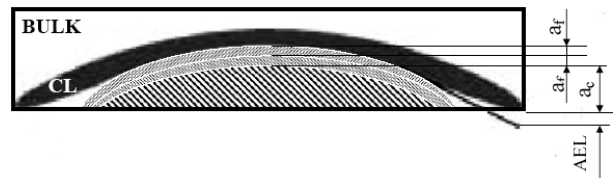


Figure 3. RGP CL design and material removal stages in the turning process

Authors assume that the change of surface topography caused by extended wear, including protein and lipid deposits, is interesting for investigation.

3. EXPERIMENTAL WORK

3.1 AFM tapping mode recording

Experimental work is conducted on commercial JOEL scanning probe microscopy – JSPM 5200 (Fig. 4), that can be configured by merely changing the tip. In general, JSPM 5200 has three different AFM modes used for topography imaging; these are the non-contact, contact and tapping mode, according to [5].



Figure 4. JOEL scanning probe microscopy – JSPM 5200 [5]

The tapping mode is used on account of its ability of non-destructive high-resolution imaging of soft and fragile samples in ambient environment. The tip is alternately placed in contact with the surface, so as to provide high resolution, and then lifted off the surface in order to avoid dragging across the sample. In tapping mode AFM, the cantilever is excited into resonance oscillation with a piezoelectric driver in ambient air at or near its fundamental flexural resonance and with free air amplitudes. The interaction with the surface (tapping) leads to energy loss and reduced oscillation amplitude. The oscillation amplitude is used as a feedback signal to measure topographic variations of the sample, as explained in [6].

In phase imaging, the phase lag of the cantilever oscillation, relative to the drive signal, is simultaneously monitored with topography data, given in [7]. As the phase lag is influenced by energy dissipation experienced during the oscillation cycle, it is very sensitive to material properties and local variations in mechanical properties. Since phase imaging highlights edges and is not affected by large-scale height

differences, it provides clearer observation of fine features that can be obscured by rough topography.

The contact lens inner surface topography image is recorded in tapping mode AFM in order to investigate changes in surface roughness. The measurement report is shown in Figure 5. RGP CL was not clean before measurements, in order to acquire relevant information about disturbing factors on surface layers. In addition, the recorded area is near to CL diameter edge, since the bubble appears in that region.

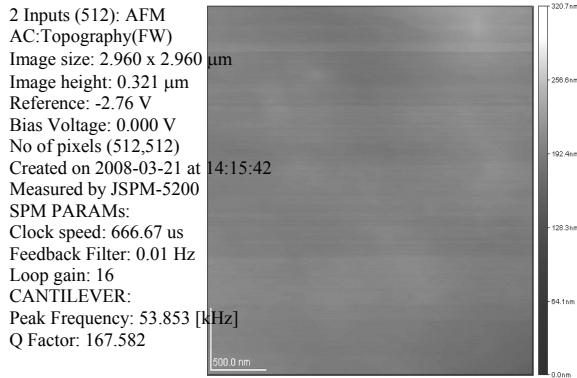


Figure 5. AFM tapping mode measurement report

By mapping out the phase of the oscillating cantilever, phase imaging goes beyond simple topographical mapping. The reason for additional phase image recording is the need for additional information about surface condition after an extended time of RGP CL wear. Both tapping mode topography and phase imaging are shown in Figure 6.

Careful observation of topography image shows the area representing the spacing of radial grooves on polymer surface. The manufactured surface is represented by impressions from a chaotic manufacturing process as turning by diamond tool that produced the circular pattern of lay of direction.

The phase image has a different appearance compared to topography image. It is obvious that phase image provides complementary information that can be observed as hay-like structures on the surface. Such differences between topography and phase images are due to material property differences on the lens surface. The appearance of fine structure in phase images complements the sensitivity to material properties, including contaminants, viscoelasticity, and regions of high and low surface adhesion or hardness. In this case, phase imaging complements lateral force microscopy, providing additional information more rapidly.

The phase image shows the presence of unexpected structures that are clearly different in their material properties from the surrounding area. These features are not present in the topography image of the lens. A likely source of the contrast in the phase image is the protein and lipid deposit formed from tears on which the lens was floating before being imaged by the JSPM 5200.

3.2 Fractal analysis by “skyscrapers” method

Fractal analysis consists of six steps that are explained in this section and shown in Figure 7.



Figure 6. Topography image (up) and phase image (down)

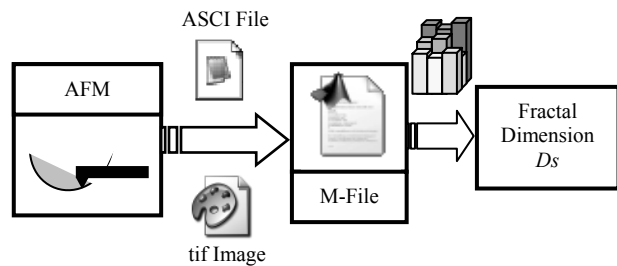


Figure 7. Scheme of data transition from AFM recording to fractal dimension calculation

The first step consists of importing AFM recorded surface data in Matlab software for further analysis. The topographic image recorded in tapping mode AFM is imported in Matlab as an image in tiff format accompanied by ASCII file. Image pixels are identified by their x and y position, while the gray-scale function is the z dimension. The image in tiff format consists of 512×512 pixels, shown in Figure 5, while the ASCII file contains 262144 five-digit numbers. That tiff image is considered as an intensity image type, and represents

```

733 40657 40602 40587 40548 40455 40484 40478 40344 40329 40335
11527 41571 41633 41730 41832 41941 42007 42079 42159 42147 4215
5 40057 40035 40068 40106 40083 40054 40032 40071 40068 40043 40
532 40566 40553 40505 40465 40444 40436 40386 40237 40276 40331
11507 41527 41482 41621 41744 41854 41919 41977 42029 42124 4220
2 39713 39681 39713 39762 39791 39807 39822 39864 39884 39890 39
581 40618 40547 40508 40483 40473 40436 40382 40300 40353 40401
11490 41522 41482 41563 41653 41752 41857 41938 41991 42070 4214
3 39336 39288 39311 39367 39458 39500 39527 39585 39656 39730 39
766 40707 40559 40543 40533 40503 40442 40395 40392 40435 40456
11453 41510 41520 41522 41571 41663 41810 41914 41972 41995 4204
3 39329 39252 39288 39370 39475 39522 39543 39557 39666 39816 39
735 40697 40578 40566 40539 40466 40386 40325 40308 40302 40300
11318 41390 41455 41472 41542 41663 41781 41850 41865 41886 4195
2 39650 39572 39581 39632 39731 39731 39697 39716 39796 39906 39
388 40844 40743 40716 40690 40650 40596 40540 40489 40447 40430
11437 41516 41610 41660 41697 41722 41849 41917 41917 41919 4195
3 40042 39981 39954 39957 40039 39982 39889 39936 39965 39986 40
085 41026 40944 40892 40867 40885 40874 40837 40752 40686 40660
11670 41749 41858 41942 41937 41846 41987 42062 42062 42045 4203
3 39918 39886 39897 39927 39965 39943 39915 39991 40013 40002 40
019 40978 40940 40854 40791 40780 40801 40798 40727 40687 40652
11841 41910 42033 42102 42157 42196 42265 42302 42302 42313 4234
5 39737 39715 39741 39773 39759 39776 39805 39821 39841 39859 39
998 40963 40914 40836 40767 40719 40718 40711 40672 40633 40591
11911 41990 42082 42120 42179 42257 42274 42312 42374 42398 4242
3 39550 39529 39549 39568 39518 39567 39633 39548 39567 39636 39
000 40965 40878 40826 40768 40685 40639 40611 40607 40556 40510
11925 42023 42070 42070 42103 42170 42157 42217 42362 42362 4238
7 39638 39616 39584 39578 39687 39688 39635 39565 39555 39574 39
969 40943 40856 40779 40718 40678 40675 40663 40616 40546 40546
11961 42056 42157 42198 42280 42352 42417 42475 42475 42475 4250
7 39589 39584 39541 39520 39636 39626 39561 39505 39500 39500

```

```

1 %% image from ASC file
2 %load ASC file%
3 dataAFM=load('CLO02-zoom.asc');
4 %matrix 512x512 from dataAFM%
5 rgbimg = zeros(512,512);
6 i=1;
7 for m = 1:512
8     for n = 1:512
9         rgbimg(m,n) = dataAFM(i);
10        i=i+1;
11    end
12 end
13 img512=uint16(rgbimg);
14 %% image from img512
15 %matrix 256x256 from matrix 512x512%
16 a = zeros(512,256);
17 b = zeros(512,256);
18 for m = 1:512
19     for n = 1:256
20         i=idivide ((n+2),int16(2),'floor');
21         a(m,i) = img512(m,n) + img512(m,n+1);
22         b(m,i) = idivide(a(m,i),int32(2),'round');
23     end
24 end
25 aa = zeros(256,256);
26 bb = zeros(256,256);
27 for nn = 1:256
28     for mm = 1:256
29         i=idivide ((mm+2),int16(2),'floor');
30         aa(i,nn) = b(mm,nn) + b(mm+1,nn);
31         bb(i,nn) = idivide(aa(i,nn),int32(2),'round');
32     end
33 end
34 img256=uint16(bb);

```

```

1 %% skyscrepers Area for top square size 1
2 %skyscrepers Area for img512 %
3 rightside512 = zeros(511,511);
4 downside512 = zeros(511,511);
5 ela512=zeros(511,511);
6 for m = 1:511
7     for n = 1:511
8         rightside512(m,n) = abs (img512(m,n)- img512(m,
9         downside512(m,n) = abs (img512(m,n)- img512(m+1,
10    end
11 end
12 for m=1:511
13     for n=1:511
14         ela512(m,n)=1^2 + 1*(rightside512(m,n)+downside
15    end
16 end
17 area512 = sum(sum(ela512));
18 %%

```

Figure 8. Partial scene of ASCII file and Matlab code for skyscrapers method

512-by-512 matrix of 8-bit integers that are linearly scaled to produce colormap indices in range [0, 255].

In the second step ASCII data is modified into 512-by-512 matrices using Matlab custom-made procedure for numbers conversion in 16-bit integers (step 2 shown in Figure 8). Such a matrix represents an intensity-type image with gray-scale colormap, where the range of values is [0, 65535]. The image generated from the ASCII file is more sensitive compared to the tiff image. Consequently, the gray-scale 16-bit image is modified for skyscrapers area calculation.

Skyscrapers analysis was originally suggested by Caldwell for fractal dimension calculation of digitized mammography. Pixels that constitute an image can be considered as skyscrapers, the height $z(x,y)$, represented by intensity of gray. The surface area of image A, referring to (1), is obtained by measuring the sum of top squares that represent skyscrapers' roofs and the sum of exposed lateral sides of skyscrapers, according to [8]. The roof of skyscrapers increases subsequently by adjacent pixel grouping and the intensities of gray are averaged. The square size ε is 2^n .

$$A(\varepsilon) = \sum \varepsilon^2 + \sum \varepsilon [|z(x,y) - z(x+1,y)| + |z(x,y) - z(x,y+1)|] \quad (1)$$

In the third step, the square size increased consecutively (1, 2, 4, 8, 16, 32) by adjacent pixel grouping, and gray levels are averaged using the Matlab custom made procedure, shown in step 3 in Figure 8. The first four images ($\varepsilon = 1, 2, 4, 8$) are shown in Figure 9.

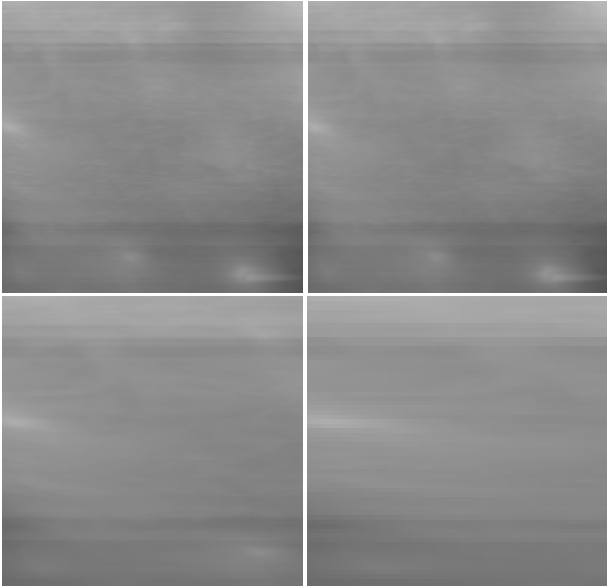


Figure 9. Images with square size $\varepsilon = 1, 2, 4, 8$

In the fourth step, the surface area A for each of the images generated in the previous step is determined referring to (1). The Matlab custom made procedure, shown in step 4 in Figure 8, results in pairs (A, ε) .

Calculated values for image area vs. square size (A, ε) are presented in a double-log graph as the fifth step. The dots are arranged along the straight line and shown in Figure 10.

This type of appearance for area and scale relationship indicates the existence of a power law between the two measures generated from the measured

surface. The power law proves the fractal behaviour of the manufactured surface with the tear component on it.

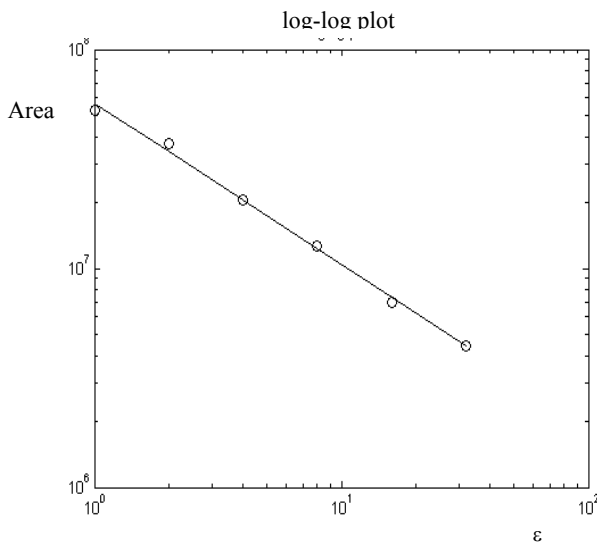


Figure 10. Log-log graph of image area vs. square size $\varepsilon = 1, 2, 4, 8, 16, 32$

Linear regression is used for fitting the plot in Curve Fitting Toolbox mode (toolbox window is shown in Figure 11). The fitting process results in a linear equation. The slope is determined from this equation.

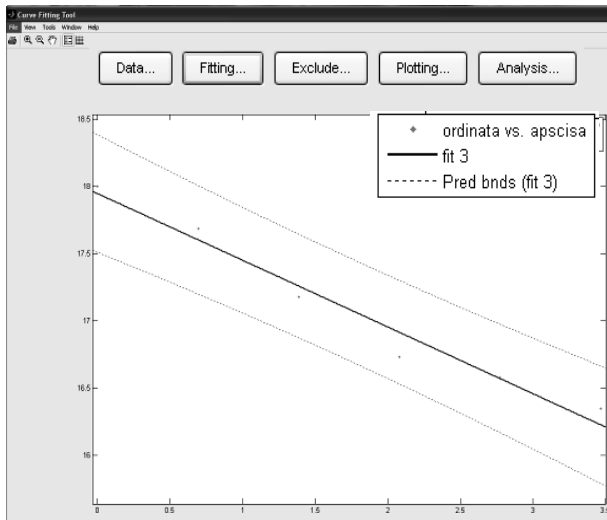


Figure 11. Data fitting using Matlab Curve fitting toolbox

The custom-made procedure for fractal dimension calculation based on “skyscrapers” method is generated using the image processing toolbox, as well as the custom-developed algorithm as the sixth step. Matlab code is shown in Figure 12.

According to [3], the fractal dimension D can be generated from (2) for Hausdorff-Besicovitch dimension where $N(\varepsilon)$ is the number of self-similar structures of linear size ε needed to cover the entire structure. Number $N(\varepsilon)$ can be represented as shown in (3) and used for the area vs. square size relationship (4) resulting in equation (5). By logarithming (5) results in a linear equation, expressed as (6). Fractal dimension D is obtained from the slope, determined in step six by using (6) in the custom-made procedure for calculation shown in Figure 10.

```

4 - a=log(A);
5 - b=log(B);
6 - % Using "curve fitting tool" window for a vs.b data set
7 - % get polynomial linear fit: a=p1*(b)+p2
8 - % Result for fitting process find in "fittedmodel2"
9 - % Linear model Poly1:fittedmodel1(x) = p1*x + p2
10 - % (95% confidence bounds)
11
12 - %Let's calculate the fitted values at every b=log(B) value
13 - y=fittedmodel2.p1*b+fittedmodel2.p2;
14 - %Plot the log-log values
15 - figure, plot(log(B),y)
16 - hold on
17 - plot(log(B),log(A),'ro')
18 - title('log-log values')
19 - xlabel('log(B)');
20 - ylabel('log(A)');
21 - %Real values in loglog plot
22 - Y=exp(y);
23 - figure, loglog(B,Y)
24 - hold on
25 - loglog(B,A,'ro')
26 - title('loglog plot')
27 - xlabel('B');
28 - ylabel('A');
29 - %Plot real values
30 - figure, plot(B,A,'ro')
31 - hold on
32 - plot(B,Y)
33 - title('Real values')
34 - xlabel('B');
35 - ylabel('A');
36 - %fractal dimension calculation D
37 - % slope p1=2-D
38 - p1=fittedmodel2.p1;
39 - D=2-p1;
40 - %%

```

Figure 12. Matlab code for fractal dimension calculation from slope using “curve fitting tool”

$$D = \lim_{\varepsilon \rightarrow 0} \frac{\log N(\varepsilon)}{\log \frac{1}{\varepsilon}} \quad (2)$$

$$N(\varepsilon) = c_1 \cdot \varepsilon^{-D} \quad (3)$$

$$A(\varepsilon) = N(\varepsilon) \cdot \varepsilon^2 \quad (4)$$

$$A(\varepsilon) = c_1 \cdot \varepsilon^{2-Ds} \quad (5)$$

$$\log A = (2 - Ds) \log \varepsilon + c \quad (6)$$

The fractal dimension generated for topography image shown in Figure 5, by skyscrapers method, is $Ds = 2.7356$.

4. CONCLUSION

The rapidly growing list of phase imaging applications [7] includes characterization of composite materials, mapping of surface friction and adhesion, and identification of surface contaminations. Phase imaging promises to play an important role in the ongoing study of material properties at the nanometre scale. Although there is currently no simple correlation between phase contrast and a single material property, the example shown in this paper demonstrates that phase imaging provides valuable information regarding the surface properties. In the given RGP CL case, the phase image confirms protein and lipid deposits that generally cause surface roughness in function. Original surface roughness changes during cleaning and wearing processes and examination of real surface roughness could ensure insight into functional behaviour.

Mandelbrot claimed that nature has a fractal face and scholars proved that engineering surfaces have fractal geometry. Compilations of a man-made surface with a tear component on it also show fractal behaviour, proven by power law of area vs. scale relationship that is obvious in Figure 9. In this paper the “skyscrapers” method is applied for calculating the fractal dimension of such surface. The fractal dimension of RGP CL inner surface is chosen for observation, as an appropriate surface roughness parameter. According to [9] a surface with fractal dimension 2.5 would be the optimum as an engineering surface for certain applications. RGP CL surface topography with deposits has a calculated fractal dimension $D_s = 2.7356$, and can be considered as inappropriate, meaning too rough for adequate adhesion property. This conclusion is in accordance with an ophthalmologist's observation of low adhesion between inner RGP CL surface and tear film.

ACKNOWLEDGMENTS

This paper is a part of the research programme: *Flexible Automation and Implementation of Intelligent Manufacturing Systems in Sheet Metal Production*, financed by the Government of the Republic of Serbia, Ministry of Science and Technological Development, Grant 14031, (2008-2010).

The authors would like to thank partners from OPTIX d.o.o. in Zemun for providing insight in the lens manufacturing process, and for the video record of worn-out RGP CL in eye.

The experimental work of tapping mode recording on JOEL scanning probe microscopy – JSPM 5200 is done in NanoLab at the University of Belgrade, Faculty of Mechanical Engineering.

REFERENCES

- [1] Bruinsma, G.M., Rustema-Abbing, M., de Vries, J., Brusscher, H.J., van der Linden, M.L., Hooymans, J.M.M. and van der Mei, H.C.: Multiple surface properties of worn RGP lenses and adhesion of *Pseudomonas aeruginosa*, *Biomaterials*, Vol. 24, No. 9, pp. 1663-1670, 2003.
- [2] Kim, S.H., Opdahl, A., Marmo, C. and Somorjai, G.A.: AFM and SFG studies of pHEMA-based hydrogel contact lens surfaces in saline solution: adhesion, friction and the presence of non-crosslinked polymer chains at the surface, *Biomaterials*, Vol. 23, No. 7, pp. 1657-1666, 2003.
- [3] Aracic, B.: *Machined Surface Modelling Using Fractal Geometry*, MSc thesis, Faculty of Mechanical Engineering, University of Belgrade, Belgrade, 2001, (in Serbian).
- [4] Bojovic, B., Kalajdzic, M., Miljkovic, Z. and Babic, B.: Fractal approach for substrates surface topography image evaluation, in: *Proceedings of the 3rd International Conference on Manufacturing Engineering (ICMEN)*, 01-03.10.2008, Kallithea of Chalkidiki, Greece, pp. 443-452.
- [5] <http://www.jeol.com>.
- [6] Prater, C.B., Maivald, P.G., Kjoler, K.J. and Heaton, M.G.: Tapping mode imaging application and technology, *Metrology & Instrumentation Application Notes*, AN04, <http://www.veeco-europe.com>.
- [7] Babcock, K.L. and Prater, C.B., Phase imaging: beyond topography, *Metrology & Instrumentation Application Notes*, AN11, <http://www.veeco-europe.com>.
- [8] Chappard, D., Degasne, I., Hure, G., Legrand, E., Audran, M. and Basle, M.F.: Image analysis measurements of roughness by texture and fractal analysis correlate with contact profilometry, *Biomaterials*, Vol. 24, No. 8, pp. 1399-1407, 2003.
- [9] Russ, J.C.: Fractal dimension measurement of engineering surface, *International Journal of Machine Tools and Manufacture*, Vol. 38, No. 5-6, pp. 567-571, 1998.

ФРАКТАЛНА АНАЛИЗА AFM СНИМАКА ПОХАБАНЕ УНУТРАШЊЕ ПОВРШИНЕ КОНТАКТНОГ СОЧИВА

Бојица Бојовић, Зоран Миљковић, Бојан Бабић

Интересовање за технологију површина биоматеријала подстакло је истраживање унутрашње површине гас-пропусних контактних сочива, уз коришћење скенирајућег микроскопа за снимање. Топографски и фазни снимци су прикупљени ради испитивања површинске хрпавости и својстава након продуженог периода ношења контактнoг сочива. Анализа се заснива на фракталном приступу примењеном у *Matlab* окружењу за анализу слике. Фрактална димензија одређена „методом небодера“, је коришћена за идентификацију и додатно појашњење функционалног понашања површине. Аутори су желели да истакну да је време ношења гас-пропусних сочива комерцијална категорија у погледу учесталости замене сочива и да само значајне промене својстава површине чине замену неопходном.